Interannual Change in Mode Waters: Case of the Black Sea

Originally published in:
Journal of Geophysical Research: Oceans 126(2), https://doi.org/10.1029/2020JC016429

JGR Oceans

RESEARCH ARTICLE
10.1029/2020JC016429

Interannual Change in Mode Waters: Case of the Black Sea

Emil V. Stanev[1,2,3], **and Boriana Chtirkova**[2,3,4]

[1]Institute of Coastal Research, Helmholtz-Zentrum Geesthacht, Geesthacht, Germany, [2]Department of Meteorology and Geophysics, Faculty of Physics, Sofia University "St. Kliment Ohridski", Sofia, Bulgaria, [3]Research Department, Sofia University St. Kliment Ohridski, Sofia, Bulgaria, [4]Institute for Atmospheric and Climate Science, ETH Zurich, Zurich, Switzerland

Key Points:

- Three cold water formation events resulted in three different mixing pathways in the upper pycnocline
- The density ratio decreased three times during the last 15 years, revealing the decreasing impact of temperature on stratification
- The horizontal patterns of potential vorticity below $\sigma_\theta = 16$ are opposite to those above this layer

Supporting Information:

- Supporting Information S1

Correspondence to:
E. V. Stanev,
emil.stanev@hzg.de

Citation:
Stanev, E. V., & Chtirkova, B. (2021). Interannual change in mode waters: Case of the black sea. *Journal of Geophysical Research: Oceans*, *126*, e2020JC016429. https://doi.org/10.1029/2020JC016429

Received 19 MAY 2020
Accepted 13 DEC 2020

Abstract More than 6,000 profiles from profiling floats in the Black Sea over the 2005–2020 period were used to study the ventilation of this basin and the mixing pathways along isopycnals. The layer of the minimum potential vorticity (PV), the Black Sea pycnostad, approximately follows the core of the cold intermediate layer, similar to the case of oceanic mode waters. However, unlike in the ocean, the horizontal patterns of PV are shaped by cyclonic gyre circulation. There is a principle difference in the probability distribution of the thermohaline properties presented in geopotential coordinates from those presented in density coordinates. In the latter case, several mixing pathways, which are not known from previous studies, dominate the ocean states. These formed after three intermittent events of cold water formation. The density ratio decreased three times during the last 15 years, revealing the decreasing role of temperature in the vertical layering of the Black Sea halocline. The basin-wide distribution of PV above $\sigma_\theta = 16$, which is where the maximum vertical density gradient appears, is opposite to the distribution below this depth. This finding suggests a complex change in the mesoscale dynamics in different layers. Comparisons of observations with data from the Copernicus Black Sea operational model demonstrate that the mixing parameterizations of models need further improvements.

Plain Language Summary Profiling floats provide nowadays a valuable information on various properties of the ocean environment. More than 38 floats were deployed in the Black Sea from 2005 to 2020, which yield more than 6,000 temperature and salinity profiles. These data are analyzed in the present paper with a focus on the ventilation and mixing pathways along isopycnals. Similarly, as in the case of the mode waters in the world ocean, the layer of the minimum potential vorticity (PV), which is known as the Black Sea pycnostad, approximately follows the core of the cold intermediate layer. However, there are strong differences from the ocean case because of the opposite (cyclonic gyre) circulation in the Black Sea. Because of this, the area of low PV is between the Rim Current and coast. The most striking finding was the occurrence of several mixing pathways, which changed after each intermittent event of cold water formation. In the past 15 years, density ratio decreased three times manifesting that the role of temperature in the vertical layering of the Black Sea halocline decreased dramatically. The observed changes are considered a precursor for similar changes occurring in other areas of the World Ocean.

1. Introduction

The cold intermediate layer (CIL) in the Black Sea is a layer of minimum temperature sandwiched between the seasonal thermocline and the permanent halocline. The CIL is formed in the winter as a result of strong cooling. During CIL formation, surface waters are subducted, and the subsurface layers are ventilated. The formation of cold intermediate water (CIW) is spread over large areas with regional enhancements due to specific dynamics, such as slope convection, fronts, open ocean eddies and coastal anticyclones (Akpinar et al., 2017; Capet et al., 2016; M. C. Gregg & Yakushev, 2005; Ivanov & Belokopytov, 2013; G. K. Korotaev et al., 2014; Mihailov et al., 2016; Oguz & Besiktepe, 1999; Ostrovskii & Zatsepin, 2016; Ovchinnikov & Popov, 1987; Piotukh et al., 2011; Shapiro et al., 2010, 2011; E. V. Stanev & Staneva, 2001; E. V. Stanev et al., 2003). The strong stratification in the seasonal thermocline tends to reduce vertical mixing, shielding the CIL from the warm surface water in summer.

The bottom of the upper mixed layer, which is rather variable, sets the upper boundary of the CIL. The extremely stable halocline limits the depth of convective mixing and sets the depth of penetration of the seasonal signal, thus determining the shape of the CIL. The thickness of the CIL is ~20–150 m; the depth of its core is ~40–80 m. Following convection events, cold waters spread along isopycnals away from their regions of origin. The layers below the CIL are not in direct contact with the atmosphere. Because of the weak ventilation, these layers develop anoxia.

The halocline is shallower in the basin interior and deeper along the coasts. This shape reflects the basic features of the general circulation: upwelling in the middle of cyclonic gyres and downwelling at their peripheries. The Rim Current approximately follows the continental slope and dynamically separates the two zones. Water masses have quite different characteristics on both sides; therefore, the current encompassing the entire basin is considered a major frontal zone. The intensity of the general circulation decreases in summer when mesoscale dynamics are relatively more pronounced and the anticyclonic eddies between the Rim Current and coast are stronger. This is known from observations (E. V. Stanev et al., 2000) and numerical modeling (Staneva et al., 2001). Different eddy activity explains the different pathways of oxygen intrusions along the isopycnals, which considerably affects the vertical oxygen conveyor belt (E. V. Stanev et al. 2014).

From the above short presentation of the Black Sea oceanography, it follows that the CIW has much in common with the mode waters in oceans (the North Atlantic subtropical mode water is known as the 18° water, Worthington, 1959). Mode water is defined as a layer of nearly vertically homogeneous water over a large ocean area (Hanawa & Talley, 2001). Both water masses, the CIW in the Black Sea and the 18° water in the Atlantic, are layers characterized by a reduced vertical density gradient trapped between the seasonal thermocline and main pycnocline. By storing heat and salt, they play an important role in climate variability. The residence time of the CIL of ~5 years has not changed much from the 1980s until the present. It is almost the same in the estimates of Lee et al. 2002 and E. V. Stanev et al. 2019 based on observations and compares well with those of E. V. Stanev et al. 2004 based on numerical simulations. This characteristic time is comparable with the respective time of mode waters in the oceans (2–7 years, Hanawa & Talley, 2001). In other words, these layers retain a memory of the atmospheric forcing conditions accumulated over several preceding winters.

The similarity between the CIL and the 18° water was mentioned for the first time by Blatov et al. (1984), who theoretically estimated that the CIL could play a substantial role in the balance of vorticity, primarily at synoptic scales. The similarities between the dynamics of CIL and the 18° water have been mentioned many times in the literature; two examples are the studies of Stanev and Staneva (2001) and Stanev et al. (2003). However, these authors analyzed data from numerical models. Most analyses of CIL used historical data, in which very few observations have been made in winter far from the coasts. Thus, the scarcity of observations precludes statistically sound estimates on the areas of formation and water renewal. The poor time sampling of historical data makes it impossible to capture the basin-wide seasonal and interannual variability of water mass formation with enough confidence.

Profiling floats have contributed substantially to advancing the knowledge of both the global ocean and regional basins, such as the Black Sea (Akpinar et al., 2017; G. Korotaev et al. 2006; E. V. Stanev et al., 2013). Large trends have been observed in the CIL during the last 15 years (E. V. Stanev et al., 2019), as well as changes in the thermohaline structure of the upper layers. The changes recorded in recent decades (E. V. Stanev et al., 2013) appear to occur much faster than what has been known previously (Belokopitov, 2011; V. N. Belokopytov & Shokurova, 2005). The definition of the CIL as the water layer with temperatures lower than 8°C (Blatov et al., 1984) no longer holds true because temperatures lower than 8°C have rarely been observed in recent years (E. V. Stanev et al., 2019).

The interaction between the CIL and the waters below its lower boundary is not very clear. The mixing pathways at the base of the CIL could aid in understanding this interaction; therefore, the layers around the base of the CIL are of major interest here.

The first objective of the present study is to describe the year-to-year evolution of the mixing pathways in the CIL using observations from profiling floats with a focus on the transformation of water masses in its core and below the core. The second objective is to demonstrate the similarities and differences between

the mode waters in the oceans and the CIW. To the best of our knowledge, such a comparison has not yet been done in the literature. Although some similarities and differences in the appearances of the water mass formation in the ocean and the Black Sea could seem obvious, they have not been widely explored; one example is the analysis of potential vorticity (PV) in the Black Sea. Bridging the analyses in the Black Sea with oceanic ones could aid in understanding the possible ocean-wide implications of our regional study because changes in the regimes of isopycnal and diapycnal mixing in the Black Sea can be considered to be amplified precursors of the expected changes in other areas of the world ocean. Comparisons with the results from numerical simulations are also shown, with the aim of challenging the numerical modelers to further improve mixing parameterizations, which is a very important issue for ocean basins with extremely strong vertical stratification (very weak vertical mixing).

The paper is structured as follows. In Section 1, we describe the vertical structure of the upper layer based on Argo observations. Mixing processes are addressed in Section 2 based on the analysis of θ-S relationships with a focus on their evolution in recent decades. The distribution of PV, temperature, and salinity on isopycnal surfaces below the core of the CIL is analyzed in Section 3, which is followed by a brief discussion and conclusions.

1.1. The Vertical Structure of the Upper Layers

We use the same data set as described by Stanev et al. (2019) and extend it until March 15, 2020, which is 15 full years. For details about the data set, the interested reader is referred to the above-cited work and to the supporting information. After removing some profiles with suspicious quality, the data set that we analyzed consists of 6,006 profiles of temperature and salinity. They are distributed uniformly in the deep part of the sea. Of these profiles, 1,531 were measured in winter, 1,478 in spring, 1,413 in summer, and 1,584 in autumn; that is, the seasonal distribution is relatively uniform, and the numbers are sufficient for statistical analysis.

In many classical θ-S analyses, individual or few profiles were used. Here, we present the totality of 6,006 observed profiles in a statistically meaningful way; therefore, we show in Figure 1 and, in Figure S1, the number of observations in a regular bin-size grid rather than the individual profiles. The color bar provides the number of observations in the individual bins. At each depth, the sum of the number of observations over the whole range of the respective variable range (all bins) equals the total number of profiles. The probability distribution would look the same; however, we prefer to present the number of profiles per bin to demonstrate the size of the observations. Using the same bin size for the surface and deep waters differently captures the scatter of data. The observations in the surface layers are spread over a wide range of respective properties; therefore, the blue color (low number of counts in a bin) dominates the distribution pattern. In the relatively homogenous subsurface layers, where the range of variability is small, the bins are too coarse to capture the variability (too many counts per bin); therefore, the red color is dominant. Thus, the representations on the left-hand side of Figure 1 are considered to be a compromise aiming to elucidate the major characteristics of the vertical stratification and at the same time to show the spread of data in the respective ranges of properties. The panels on the right-hand side of Figure 1 show the distribution of observations plotted in an interval of 5 s, left and right from the mean value (stretched plots), where s is the standard deviation taken as depth dependent (estimated over all the measurements at the same depth). The vertical white zero line shows the mean.

Qualitatively, Figures 1a, 1c, and 1e describe the same characteristics as those analyzed by Stanev et al. (2019) but in terms of the data distributions of potential temperature θ, salinity S, and potential density σ_θ. In the context of the analyses carried out, it is important to stress the small range of variability in σ_θ (Figure 1e) at the base of the upper mixed layer (~40 m). Above this depth, the relatively large range of density variations is explained by the large range of potential temperature (Figure 1a) due to the seasonal signal in the upper mixed layer. Below this depth, there is a large range of salinity (Figure 1c), which explains the range of density variations. This large salinity range is due to the strong horizontal gradients in the major frontal zone, which is in the area occupied by the Rim Current.

Most data at ~30 m depth are localized in a narrow temperature interval (~41% of the observations at that depth fall in the red-colored interval). However, the variability range is rather large (Figures 1a and 1b).

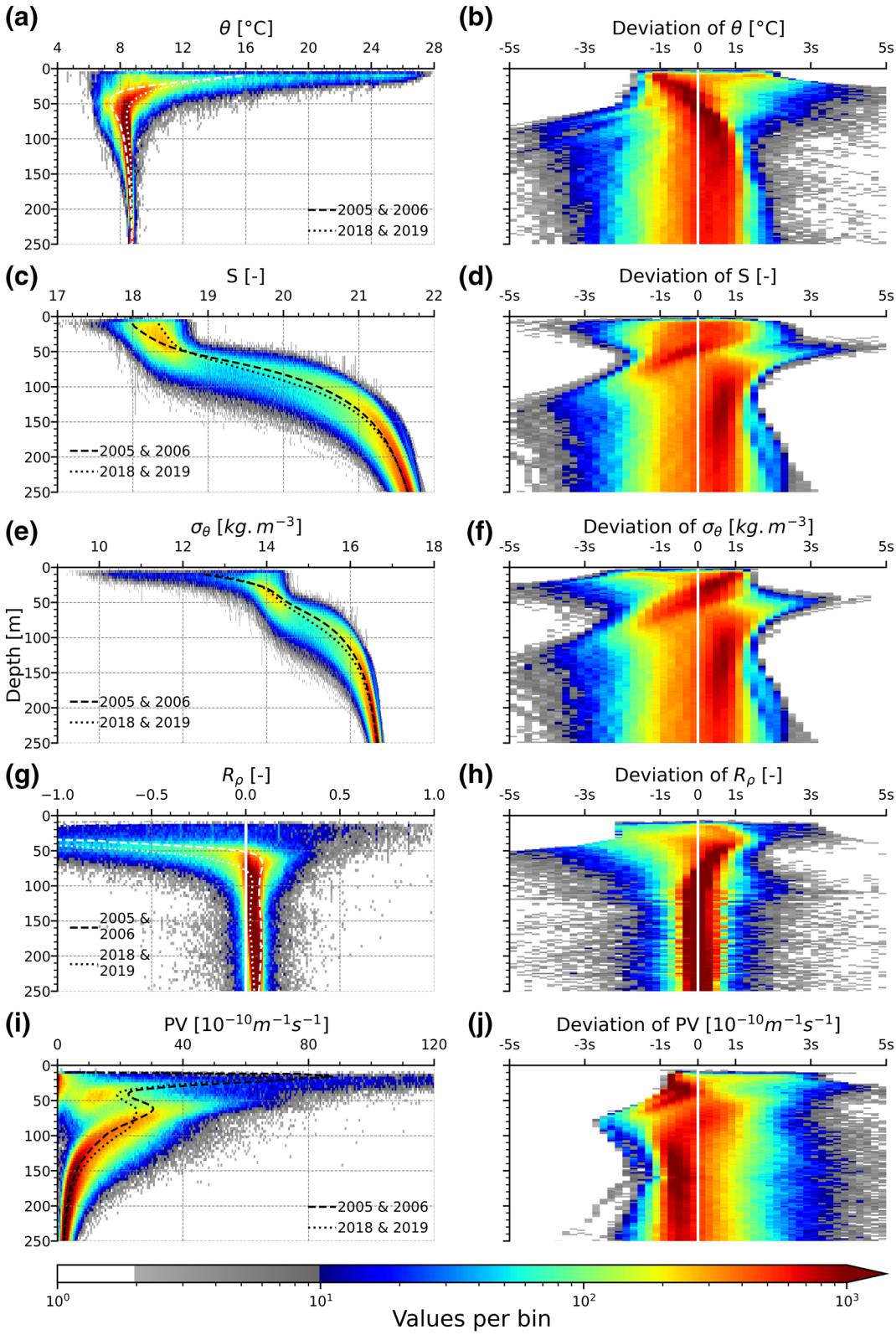
(a)
θ [°C]
(b)
Deviation of θ [°C]
(c)
S [-]
(d)
Deviation of S [-]
(e)
σθ [kg. m−3]
(f)
Deviation of σθ [kg. m−3]
(g)
Rρ [-]
(h)
Deviation of Rρ [-]
(i)
PV [10−10m−1s−1]
(j)
Deviation of PV [10−10m−1s−1]
Depth [m]
2005 & 2006
2018 & 2019
Values per bin

Because of the warm water in the seasonal thermocline, the +/−5 s interval extends over 23.5°C. In contrast with the temperature, salinity is more uniformly distributed on both sides of the respective mean salinity down to ~30 m (Figures 1c and 1d).

The density ratio $R\rho = \frac{\alpha d\theta / dz}{ßdS / dz}$, where α and ß are the coefficients of thermal expansion and salinity contraction compares the individual contributions of temperature and salinity in the density stratification. As known from earlier studies (Ozsoy et al., 1993; Stanev, 1990; E. V. Stanev et al., 2003), over most of the water column, this property is a small number (Figures 1g and 1h). The overall trend is such that temperature has a stabilizing role down to the core of the CIL (negative values of $R\rho$). Therefore, the density ratio is a very useful characteristic determining the position of the CIL as the depth where the stabilizing effect of temperature reverses (minimum temperature in the core of the CIL). In the layers below the core of the CIL, the increase in temperature with depth has a destabilizing effect (the sign of the density ratio reverses). The small values of the density ratio below the core of the CIL provide a measure of the very low contribution of temperature to density stratification.

The vertical density gradient (or Brunt-Väisälä frequency) is usually used for identifying mode water. This quantity is proportional to the PV, which is expressed as $\mathrm{PV} = \frac{f}{\sigma_\theta}\frac{\mathrm{d}\sigma_\theta}{\mathrm{d}z}$, where f is the Coriolis parameter. While the dynamics of the PV in the Black Sea have not been much addressed, many studies have focused on buoyancy frequency profiles based on ship-borne observations. PV, which is also called isopycnic PV, is a very useful characteristic since it is a dynamically conserved property through the path of a particle along isopycnals (Provost et al., 1995). It can only be changed by diabatic or frictional processes. It has long been established that in small basins such as the North Sea, high-resolution CTD profiles trace eddy signals along the thermocline caused by intrusions of low salinity waters (Badin et al., 2009). For the Black Sea, Staneva et al. (2001) explained the key role of vertical stratification in the formation of eddies in the following way. In summer, the increase in vertical stability tends to change the PV of the upper layers of the water column, resulting in a change in the ratio between the intensity of the gyre and eddy circulations compared with the winter case (E. V. Stanev et al., 2014). To our knowledge, the basin-wide dynamics of PV in the Black Sea have not been studied based on observed profile data. The large amount of such data from profiling floats provides a unique opportunity to address this issue based on observations.

The annual mean PV is at the maximum in the upper mixed layer mainly because of the strong stratification in summer (Figure 1i). The value decreases in the layers below (see the dashed lines), reaching the minimum at approximately the depths where the scatter of density profiles is minimal (~40 m). Approximately 10 m below this depth is the core of the CIL. The minimum PV at ~40 m can serve as evidence that the CIL in the Black Sea shares some similarities with the mode waters in the ocean. Minimum PV, or minimum vertical density gradient, in the world ocean is known as a pycnostad, and it usually coincides with the layer of the vertical minimum of temperature (e.g., McCartney, 1982). Obviously, Figure 1i reveals the Black Sea pycnostad as a layer between the seasonal thermocline and the main pycnocline (halocline).

The vertical distribution of PV is characterized by three zones of "concentration" of observed profiles. The large concentration layer of water with very low PV (almost zero) just below the sea surface is explained by the strong mixing in the surface layer caused by wind and wind waves in winter. However, there is a large scatter of data in this surface layer (including very high values of up to 200×10^{-10} $\mathrm{m^{-1}\ s^{-1}}$), illustrating that in most cases, the stratification is extremely strong. The second zone of concentration of profiles (high

Figure 1. Vertical distribution of (a) potential temperature, (c) salinity, (e) potential density, (g) density ratio and (i) PV in the upper 250 m (panels on the left) presented as a function of the number of samples per individual bin. A gray color is used where there are less than 10 observations per bin. Bins, in which there are fewer than two observations, are ignored (white in the color bar). A detailed representation of the distribution with an increasing property resolution in the deeper layers is shown in the respective panels on the right (b, temperature, d, salinity, f, potential density, h, density ratio, and j, PV). Vertical white lines represent the mean values and the zero value in (g). *X*-axes (Deviation) measure the standard deviation *s* of respective properties. Each bin is 2 m thick. The *x*-axis in the panels on the right is split into 50 bins, that is, each bin is 0.2 standard deviations wide. Dashed and dotted lines in the panels on the left are the means for the first two (2005 and 2006) and last two years (2018 and 2019). PV, potential vorticity.

values of the number of profiles per PV-depth bin) is the one in the core of the CIL at ~40 m, which is where the PV is low. Below the zone of maximum PV, at the base of the CIL (~70 m), PV decreases monotonically with depth because salinity stratification is weaker there (comparing Figure 1c with Figure 1i). However, the PV values in the halocline remain approximately an order of magnitude higher than the ocean values (Hanawa & Talley, 2001).

The distribution of the individual observations around the mean is not Gaussian, which is a consequence of the specific dynamics. The skewness is well demonstrated by the scatter of salinity in the main halocline, which is smaller to the right of the mean value (see the distribution at ~150 m in Figure 1d). The analysis of the distribution patterns per region shows that most of the respective observations in the area of maximum probability originate from the central parts of the gyres. This result illustrates that the distribution of salinity in the gyres is more homogenous than that over the continental slope. The larger scatter to the left of the mean value is characteristic of vigorous mixing between coastal (low salinity) and open ocean (high salinity) waters in the area of coastal anticyclones and the baroclinic front (Rim Current).

The good correlation between potential temperature and salinity in the halocline is demonstrated by the symmetric scatter of the density ratio below 100 m (Figure 1h). The low-density ratio (Figure 1g) explains why the distribution pattern in Figure 1f (density) is similar to that shown in Figure 1d (salinity). Below the core of the CIL, *PV* shows a distribution that is opposite to that of density (comparing Figures 1f and 1j); that is, a larger scatter of PV occurs to the right of the mean value. In other words, a larger PV is characterized by a larger variability range.

The dashed and dotted lines in the panels on the left in Figure 1, which show the mean vertical profiles calculated for the first and last years of the observations, support the earlier analyses of the same data, demonstrating that the vertical stratification in the Black Sea has changed dramatically in recent years (E. V. Stanev et al., 2019). What has not been addressed in this work is the impact of these trends on the density ratio and PV. As far as the density ratio is concerned, the positive mean values at ~60–70 m are much lower than what was observed by Ozsoy et al. (1993) in the summer of 1988. The mean profiles of $R\rho$ in 2018 and 2019 shifted to the deeper layers of the CIL in the last 15 years (Figure 1g). Notably, the shift to the left of the $R\rho$ profile below the CIL (a decreasing $R\rho$ trend) demonstrates the decreasing role of temperature for the vertical layering of the Black Sea halocline. The opposite trends of PV above and below 80 m at the beginning and end of the last 15-year period (Figure 1i) suggest that the recent changes in the stratification (respectively PV) have resulted in changes in the mesoscale dynamics.

To further understand the dynamics of the CIL and the respective similarities and differences with the mode water formation in the ocean, it is necessary to briefly describe the outcrops in the Black Sea (Figure 14 of E. V. Stanev et al., 2003). In the ocean, the outcropping isopycnic surfaces reach their southernmost displacement in winter and retreat to the north in summer; however, there are some important specificities in the Black Sea. (1) The outcropping in the Black Sea only occurs in (part of) the winter season and (possibly) not over the whole sea. (2) The Black Sea gyres have a rotation sign, which is opposite to that of subtropical gyres. (3) The upwelling in the Black Sea gyres is an important preconditioning factor. (4) The regional circulation and stronger cooling in some areas over the continental slope additionally shape the ventilation complexity in the Black Sea. These specificities will be analyzed later in the text, along with the regional characteristics of Black Sea ventilation.

2. Analysis of Mixing Based on the θ-S Relationship

2.1. General Concepts

Ocean mass formation starts as a diapycnal process in the upper layers followed by along-isopycnal mixing in the pycnocline. According to McDougall (1984), who analyzed the equation for the rate of change of the potential temperature on a neutral surface, the diapycnal turbulent mixing is proportional to the curvature of the θ-S curve $d^2S/d\theta^2$. A similar relationship could be formally obtained if we analyzed the equation for the rate of change of salinity. This approach is more appropriate for the Black Sea, where salinity monotonically increases with depth and temperature has a minimum in the core of the CIL. Recall that the core layers are where a vertical extremum of a property occurs (Wüst, 1935). Therefore, in the Black Sea case, the

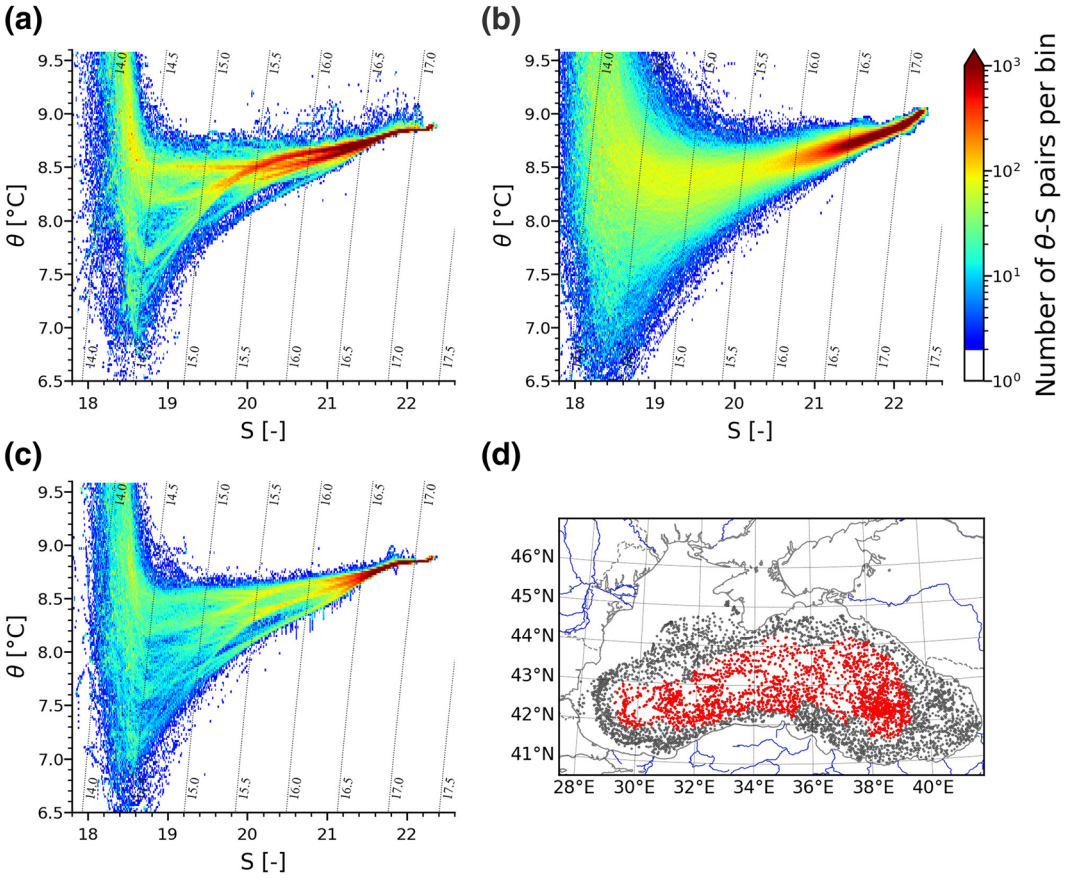

Figure 2. Distribution diagrams in the (a) θ-S space from profiling floats and (b) CMEMS reanalysis sampled in the same way (in time and space) as by the floats. (c) is the same as (a) but uses only data from the locations deeper than 2,000 m. The bin sizes are 0.02°C and 0.01 psu. Bins, in which there was only one observation, are not shown. Colors (see color bar) correspond to the number of data points in the respective T-S bins. Thin lines show several potential density isolines. (d) shows the horizontal distribution of the data used in the 15-year analysis period (red is used for the data from the locations deeper than 2,000 m). CMEMS, Copernicus Marine Environment Monitoring Service.

diapycnal mixing coefficient is proportional to $d^2\theta/dS^2$. The almost straight lines in the θ-S diagrams signify approximately constant $R\rho$ (see Figure 1g below the core of CIL). As demonstrated by Stanev (2014, 2018), curved profiles of biogeochemical variables (nonconservative) in the Black Sea may also be due to internal sources or reaction terms.

The neutral surfaces (hereafter, isopycnal surfaces will be used synonymously) are defined as surfaces where $\alpha\nabla\theta = \beta\nabla S$, and ∇ is the horizontal gradient operator. As it is well known for the ocean and for the Black Sea (S. K. Konovalov et al., 2005; McWilliams, 1983, Turgul et al., 1992; E. V. Stanev et al., 2004; 2014), the isopycnal spread (gradients) of temperature and tracers is much smaller than the respective gradients on geopotential surfaces, which is explained by the fact that the mesoscale variability (characterized by large-magnitude variations) is canceled on isopycnal surfaces. Therefore, in the Black Sea, the overall vertical stratification in the density coordinates is adequately represented by only a few vertical profiles. However, the details of the basin-wide spatial variability of water masses, as seen in density coordinates, cannot be represented by only a few vertical profiles. In our case, the number of profiles is high, which allows us to perform a deeper analysis of the temporal and spatial variability in diapycnal and isopycnal mixing.

In the analysis that follows, we will address the θ-S relationships below the core of the CIL, down to ~250 m, in more detail. Most of the discussion will focus on the vertical characteristics of the θ-S diagrams and their temporal variabilities. The spatial change in the mixing patterns on isopycnal surfaces will be addressed in Section 4.

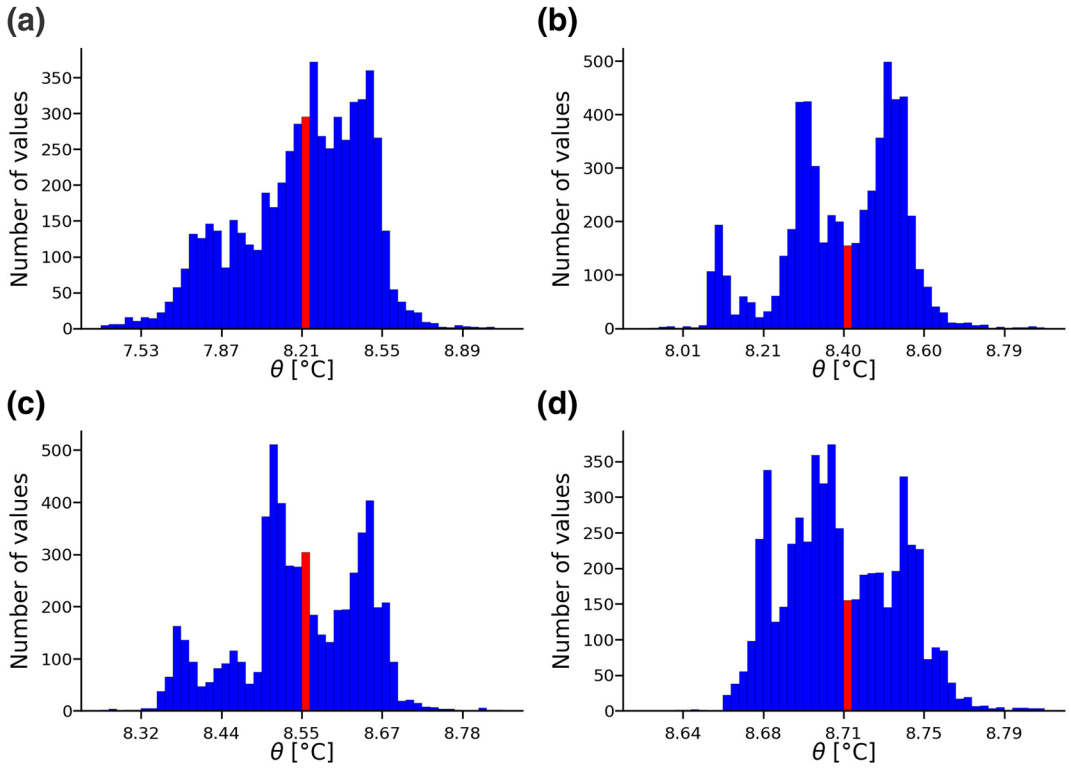

Figure 3. Histograms of potential temperature at σ_θ surfaces (a) 15, (b) 15.5, (c) 16, and (d) 16.5. The interval in which the mean potential temperature occurs is colored red.

2.2. θ-S Analysis

The distribution of all observations from the profiling floats in the whole water column presented in the θ-S plane (Figure 2a) illustrates the basic characteristics of the thermohaline structure of the CIL in the last 15 years. Only the θ-S relationships for waters colder than 9.6°C are shown, which ignores a large part of the observations in the surface layer (warmer water) but enables a better bin resolution in the intermediate and deep layers. As in Figure 1, the colors on this plot do not show individual θ-S relationships but do show their distribution on the θ-S plane. The dominant θ-S characteristics in Figure 2a are seen as maxima in the probability distribution patterns. This presentation is a good substitute for presenting individual θ-S indices with small dots; in the later presentation, dots would overlap because of the large amount of data. Isopycnals are also shown in this figure. The thermohaline properties of the deep layers, that is, the layers that fill most of the volume of the Black Sea but a very small area in θ-S space, are considered by Stanev et al. (2021).

The large scatter of data in the surface layer is consistent with the representation in Figure 1a. At the bottom of the CIL ($\sigma_\theta \sim 16.5$ kg m^{-3}), the temperature and salinity values converge in a very narrow range of θ-S indices; this range further reduces with increasing depth. The core of the cold waters is most pronounced at $\sigma_\theta \sim 14.5$. This density was used by Stanev et al. (2003) to formulate the conditions under which CIW formation occurs. Above and below the core of the CIL, the angle between the θ-S curves and σ_θ lines is the opposite, revealing the stabilizing role of temperature in the upper layers and its destabilizing role below the core of the CIL. The scatter of data with positive temperature anomalies below $\sigma_\theta \sim 15.5$ reflects the intrusions in the pycnocline, which will be addressed in a separate study.

The largest curvature of the θ-S relationships in the core of the CIL suggests that this core is the zone of maximum diapycnal mixing (see Section 3.1). The most important property of the water mass below $\sigma_\theta \sim 15.5$ is the nearly linear θ-S slope (a very small curvature). Furthermore, the very small range of θ-S indices at specific σ_θ values in the pycnocline shows the homogenization of properties on isopycnal surfaces. The most

striking feature in the θ-S distributions shown in Figure 2a is the convergence of thermohaline states along several narrow mixing pathways (bins with the most frequent appearance of θ-S pairs). In the following, we refer to these features as "mixing channels." These non-Gaussian (and multiple maxima) distributions of temperature and salinity on isopycnal surfaces are illustrated in Figure 3 for four σ_θ levels below the core of the CIL. These "mixing channels" reveal a changing distribution of properties with changing isopycnal depth (Figure 3). The comparison between Figure 3 and the panels on the right-hand side of Figure 1 shows one fundamental difference. The distributions seen in pressure coordinates have only one maximum, and all properties are characterized with a certain skewness (see also Figure S3). The presentation in the density coordinates (see for more details Figure S1) is completely different, with several maxima, and their positioning with respect to the mean is very different for the individual σ_θ levels.

The nonuniform distribution seen at specific density levels would suggest that either the CIL resided in some states most of the time during the observed 15-year period (therefore, the localized maxima in the probability distribution) or that the sampling and interpretations were not statistically credible. To exclude the second hypothesis, we sampled the output from the reanalysis provided by the Copernicus Marine Environment Monitoring Service (CMEMS) operational model (see https://resources.marine.copernicus.eu/?option=com_csw&view=details&product_id=BLKSEA_ANALYSIS_FORECAST_PHYS_007_001, last assessed on April 16, 2020, and Ciliberti et al. 2019) in the same spatial and temporal manner as the floats did (the positions of the observations are shown in Figure 2d). The result from the model (Figure 2b) was to the first order similar to the observations. The overall θ-S characteristics of the main water masses (surface, cold intermediate and deep) do not differ much between the observations and numerical simulations (comparing Figure 2b with Figure 2a). However, the "mixing channels" do not appear in the model data. Here, we remind the reader that the data from the same profiling floats have been assimilated in the operational product. To ensure that the Argo sampling did not affect the representation of numerical simulations in Figure 2b, we produced this figure by sampling the model uniformly in time and space so that the number of profiles from the model nearly equals the number of observed profiles. The two samplings show almost identical distributions, as shown in the comparison between the two panels in Figure S2.

A further possibility to misinterpret the mixing pathways would be that these features are revealing specific regional conditions. Knowing that the dynamics of the Black Sea differ greatly on the two sides of the continental slope, we replotted Figure 2a using the data from the deep ocean only (red dots in Figure 2d). The similarity between Figures 2a and 2c and the analysis presented above exclude the possibility of an incorrect interpretation of observations. Another test of consistency of data analysis was to avoid using non-homogenous in time observations by analyzing monthly-averaged profiles. The results (not shown here) almost repeat Figure 2a. Therefore, we conclude that the "mixing channels" seen in the θ-S relationships are credible features characterizing several different thermohaline states in all Black Sea areas visited by the profiling floats. If observations of the Black Sea using profiling floats are extended for the next 15 years, other mixing channels would probably appear, corresponding to the new thermohaline states.

The analysis of model data was performed only to check the robustness of the results against sampling. However, one conclusion needs to be mentioned. The model appears to be overly diffusive and does not replicate the tiny "mixing channels" seen in the observations. This comparison between the observations and numerical simulations presents a challenge for numerical modelers and indicates that further efforts are needed to adequately specify mixing parameterizations, particularly in basins with extremely strong vertical stratification (Stanev et al., 1997). The results from numerical simulations will not be discussed further in the main text because our study addresses the analysis of observations. For the interested reader, the supporting information shows some of the analyses that are discussed further in the text but are performed using the CMEMS data.

2.3. Year-to-Year Variability

The interannual variability in the world ocean associated with ENSO or NAO has time scales from 2–7 years up to decadal time scales. Talley (1996) showed that the 18° water core correlated with the NAO index. Belokopytov (1998, 2011) and Piotukh et al. (2011), who analyzed the interannual and decadal variabilities, identified comparable time scales from the Black Sea historical data. The data set that we use is only 15

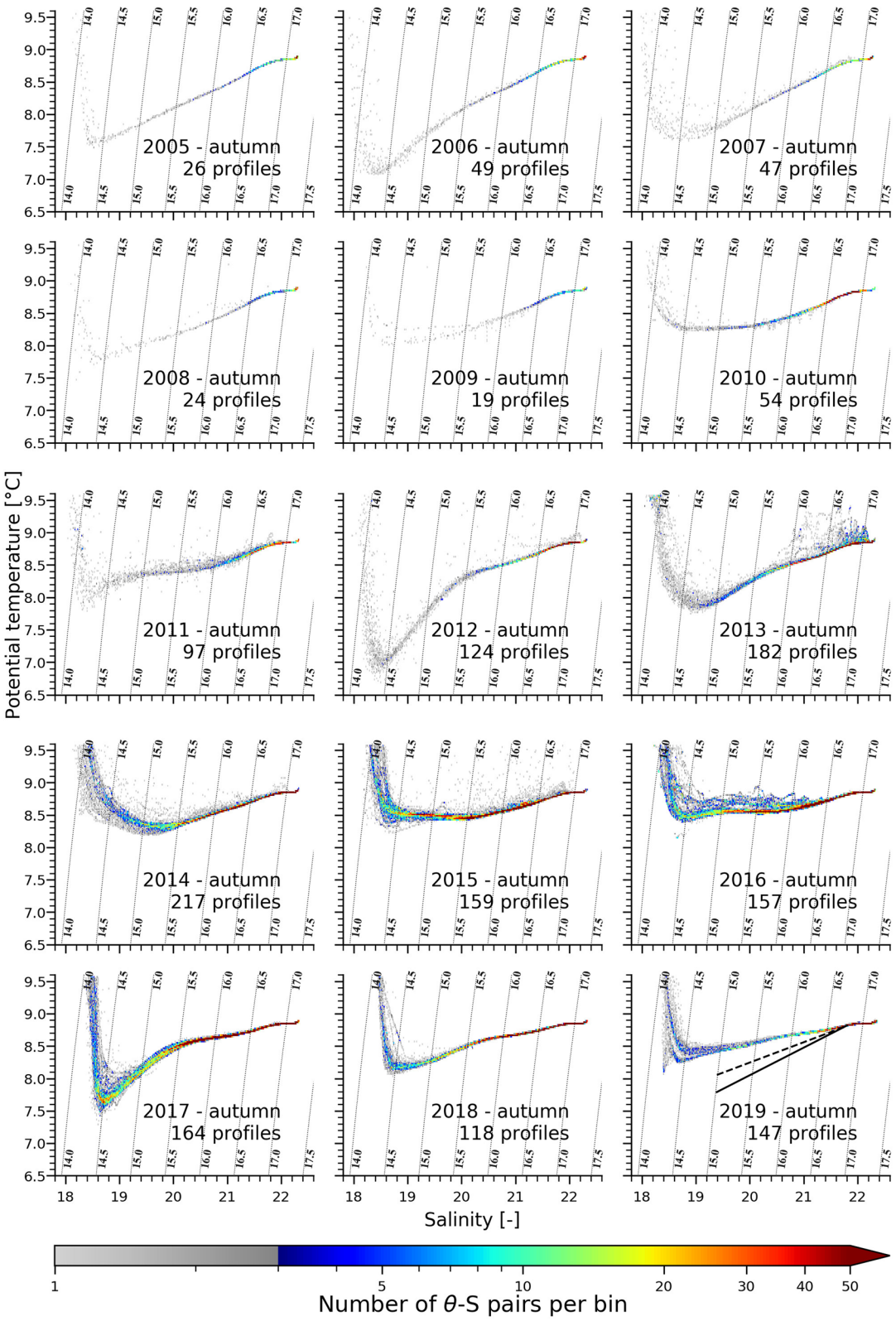

Figure 4. Autumn distribution of θ-S indices (pairs per bin) for the individual years. The almost linear parts of the 2006 and 2012 distribution plots are added to the 2019 panel with black full and dashed lines, respectively, to show the trend over 15 years. These lines are the linear regression lines. The bin size is 0.02°C × 0.01 psu. Thin lines show several potential density isolines. The number of profiles used to plot the panels in individual years is also shown.

years long; therefore, the interannual variability in the analysis to follow can be named the year-to-year variability.

To better understand the details of the θ-S distributions in Figure 2, we separately present the distributions for each autumn (October, November, December) for the entire 15-year period in Figure 4. The figures for the remaining seasons are shown in the supporting information: Figure S5 (January, February, March), Figure S6 (April, May, June) and Figure S7 (July, August, September). We present the autumn situation in the main text because this season is the most distant from the period of winter convection and better reveals the established structure of the CIL after major events of water mass formation, which occurred in 2006, 2012, and 2017.

Waters in the Black Sea, which are deeper than the CIL, are considered to be formed by two end-member mixing of the CIW and waters originating from Bosphorus (J. W. Murray, 1991; J. W. Murray & Yakushev, 2006). One can now question the robustness of these end-members. It is instructive to first estimate the changes in θ-S indices due to seasonal cycles. The comparisons of the θ-S distribution curves in individual seasons (one example for 2013 is given in Figure S4) demonstrate that the range of the seasonal variations in the core of the CIL is approximately twice as small as the range of interannual changes (see Figure 4 and Figures S5–S7). Below $\sigma_\theta \sim 15.5$, the seasonal changes are negligible (the data spread associated with the warm Bosporus intrusions is more pronounced in the deeper layers); therefore, the major interest in the following will be on the year-to-year change in these layers.

It was only in 2006, 2012, and 2017 that the temperatures in the core of the CIL dropped below 7.5°C (Akpinar et al., 2017; E. V. Stanev et al., 2019). From 2006 until 2011, the core temperature continuously increased, reaching values warmer than 8°C. The convective event in 2012 cooled the waters in the core below 7°C, which was around the typical temperature values for the past periods. Another period of continuous warming of the core, up to 8.4°C, followed after 2012 until the last event in 2017. One conclusion from this short chronology is that the CIW is a variable end-member, and any analyses on the thermodynamics of the upper layers have to adequately address the interannual variability.

At the beginning of the period, which we analyze here (2005), the θ-S indices showed a linear trend between the θ-S values characteristic of the core of the CIL and those at $\sigma_\theta = 16.75$ (T~8.8°C, S~21.8). The slope of the distribution curve at the base of the CIL (between $\sigma_\theta = 16$ and $\sigma_\theta = 16.75$) remained nearly constant from 2005 to 2008 (the thick straight line in the 2019 panel of Figure 4 is parallel to the distribution curves in this interval throughout this period). The steepness of the θ-S curves at the bottom of the CIL decreased dramatically in 2012, which is just after the second convection event. This result would suggest that the latter triggered a substantial change in the regime of mixing. The mixing curve was no longer a straight line. Its steepness changed considerably at $\sigma_\theta = 15.5$, which would indicate substantial diapycnal mixing at this level. After the event in 2012, the slope of the mixing curve changed substantially in comparison to the situation at the beginning of the analyzed period. The linear parts of the mixing curves in 2006 and 2012 are added in black in the 2019 panel of Figure 4 to compare the actual state against the past thermohaline states.

Each of the three thermohaline states schematically presented in the 2019 panel of Figure 4 is reflected in the composite diagram in Figure 2a and could be considered a response to intense water mass formation during 2005–2020. The slope of the density lines is α/β (on the neutral surfaces, $\alpha\theta_z = \beta S_z$), while the slope of the θ-S distribution lines is θ_z/S_z. The three different slopes plotted in the 2019 panel of Figure 4 reveal the diminishing trend of the $R\rho$ profiles at the base of the CIL (see also Figure 1g). This trend indicates a reduction in the role of temperature in recent years. It is easy to provide a measure of the change in $R\rho$. The salinity difference between the water in the core of the CIL and at its base changes slightly during the 15-year period; therefore, we will neglect it. However, the difference between the temperatures in the core and at $\sigma_\theta = 16.75$ were 1.3°C and 0.4°C at the beginning and end of this period, respectively. This would result in a ratio of 3.25 between the respective $R\rho$ numbers. The conclusions are listed as follows: (1) by affecting $R\rho$, the recent thermohaline changes could have resulted in a decrease in isopycnal mixing; and (2) these changes not only appeared in the surface layers but also propagated deeper in the Black Sea halocline.

We will end this part with a reminder to interested readers that a parallel set of figures produced by an operational model is presented in the supporting information (see Figures S8–S11). While the overall slope of

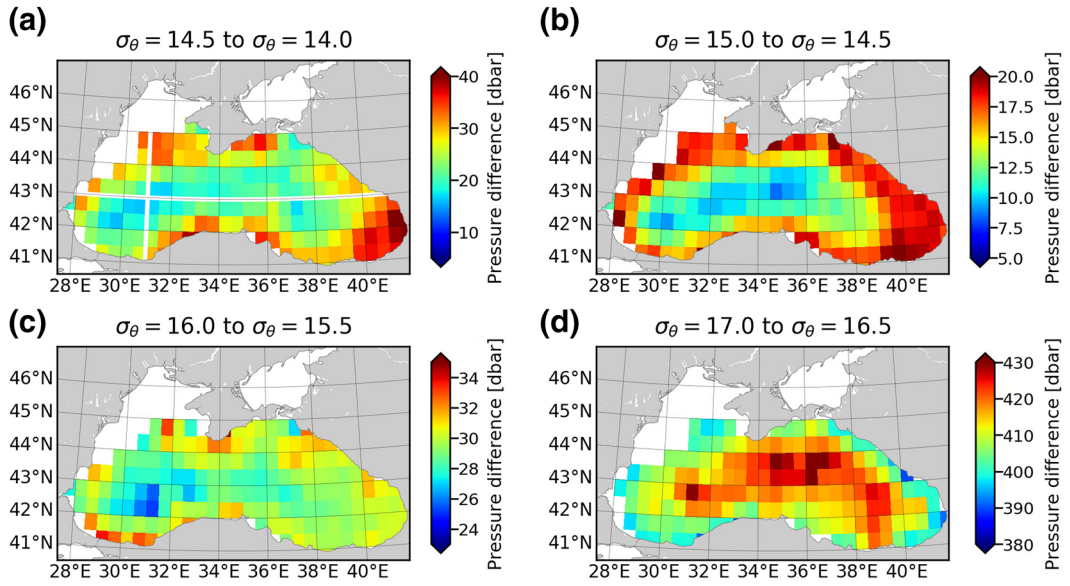

Figure 5. Thicknesses of layers between σ_θ surfaces (a) 14.5–14, (b) 15–14.5, (c) 16–15.5, and (d) 17–16.5 averaged for the 2005–2020 period in 0.5° squares. The parallel and meridian plotted with thick white lines show the positions of the sections presented in Figure 7.

the mixing curves in the lower part of the CIL does not differ much from the observed slopes, the scatter in the CIL provides room for further improvement of the simulation quality.

3. Spatial Variability in the Properties on Isopycnal Surfaces

Addressing the spatial variability on the isopycnal surfaces is a challenge because in the lower part of the CIL, the range of temperature change is very small (e.g., less than 0.15°C at $\sigma_\theta = 16.5$, see Figure 4), that is, the signal-to-noise rate is low. This rate would further decrease if we remove the trend associated with the interannual change. Here, we remind readers that in a steady-state ocean without diapycnal mixing in the ocean interior or at the boundaries or without double diffusion, θ has to remain uniform on the neutral surface (T. J. McDougall, 1984). The real case, which we consider to be neither of these, is that the permanent upwelling in the cyclonic gyres adds to the diapycnal mixing.

The mode water formation is controlled by the permanent fronts in such a way that in the North Atlantic, this water mass occurs on the low-density side of the front. The shallower depth of isopycnals along the front preconditions the outcropping. The regions with thicker layers with the same density (e.g., the subtropical gyres) are to the right side of the front looking in the direction of the main current (North Atlantic Current). This concept can be applied to the formation of cold waters in the interior of the Black Sea, where the upwelling in the cyclonic gyres pinches the isopycnal surfaces toward the ocean surface, thus preconditioning outcropping. However, the area of thicker layers with the same density at the low-density side of the front in the Black Sea is squeezed in the narrow space between the Rim Current and the coast, or between the Rim Current and the shelf in the North Western Black Sea.

All data have been mapped onto 0.5° squares, which allows for ~30 profiles per box. First, we will analyze the thickness of layers between σ_θ surfaces 14 and 17 (Figure 5). The horizontal distribution of PV shows similar (just opposing) patterns to the one shown in Figure 5 and will not be presented in detail. The isopycnal surface $\sigma_\theta = 14$ outcrops every year (see Figure 4d of E. V. Stanev et al., 2019 and Figure S12); therefore, the average thickness of the layer between $\sigma_\theta = 14$ and $\sigma_\theta = 14.5$ for the 15-year period is only ~20 m in the interior Black Sea. In the coastal areas of the southern and eastern Black Sea, the thickness doubles (~40 m). The layer thicknesses between σ_θ surfaces 14.5–14, 15–14.5, 15.5–15, 16–15.5, 16.5–16, and 17–16.5 are 31, 16, 18, 30, 80, and 403 m, respectively. The standard deviations for the same layers are 5, 2, 2, 2, 5, and 8 m, that is, these

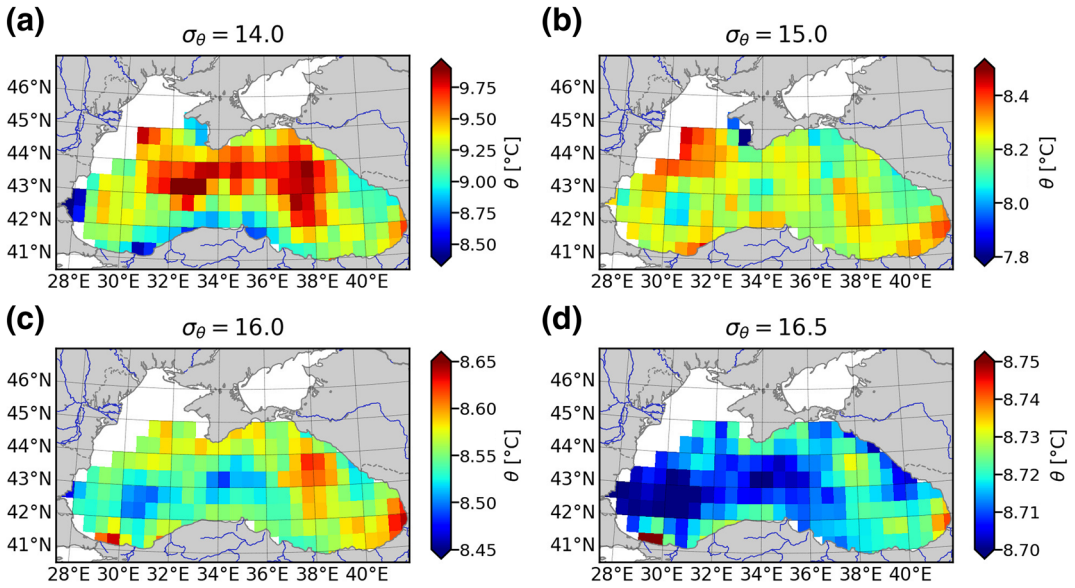

Figure 6. Temperatures at σ_θ surfaces (a) 14, (b) 15, (c) 16, and (d) 16.5 averaged for 15 full years during 2005–2020 in 0.5° squares.

numbers are considerably smaller than the range of respective thicknesses. Although the "signal versus noise" ratio is not a very large number, the overall statistical credibility of the results presented in the following is ensured as far as the annual mean situation for the entire period is concerned. Unfortunately, the coverage is not sufficient to produce statistically stable results for seasonal or even for the year-to-year variabilities in the basin-wide properties. The seasonal mean layer thickness is shown in the supporting material (Figures S12–S15).

The small thickness of the isopycnal surfaces in the interior of the cyclonic gyres dominates the horizontal distribution from the top of the CIL down to $\sigma_\theta = 16$ (Figures 5a–5c). This pattern is explained by the upwelling in the cyclonic gyres, which displaces the isopycnal surfaces in the basin interior upwards; therefore, they become thinner. The largest gradients occur in the frontal area, which is approximately on the continental slope. In these areas, PV, which is inversely proportional to the layer thickness, also shows the largest gradients. This finding suggests an impact of these gradients on the mesoscale dynamics because the latter are constrained by the PV. We remember that the PV values in the Black Sea layers considered here are approximately an order of magnitude higher than the ocean values.

The distribution of the layer thickness between $\sigma_\theta = 17$ and $\sigma_\theta = 16.5$ is the opposite of those in the layers above, that is, the layer is thicker in the basin interior and thinner along the coast. The trend reversal occurs at approximately $\sigma_\theta = 16$. At this isopycnal surface, PV is nearly uniform basin wide with a value of $6{,}21.10^{-10}$ m^{-1} s^{-1}. Between the σ_θ surfaces 14.5–14, the difference between PV in the basin interior and in the coastal zone is approximately twice the mean value. Below $\sigma_\theta = 16$, this difference is a~10% of the mean. Obviously, the generation and propagation of eddies in individual layers should be affected by the reversal of PV at $\sigma_\theta = 16$. This trend works in combination with the seasonal changes in PV. In summer, the increase in the vertical stability in the seasonal thermocline tends to change the PV in such a way that an anticyclonic rotation trend is generated to conserve the vorticity. This reduces the cyclonic circulation in the interior. In the coastal area (this is the area dominated by coastal anticyclones), this change tends to further enhance the anticyclonic circulation. This seasonality could explain the decrease in the ratio between the intensities of gyre and eddy circulations in summer compared with the winter case (E. V. Stanev et al., 2014). As suggested by the results in Figure 1i, the PV trend in the last 15 years can also affect the mesoscale variability because the difference between PVs in the upper 80 m and below decreased.

The distributions of potential temperature and salinity on constant potential density surfaces are not independent; therefore, we will analyze only θ (displaying both θ and S is redundant). The annual mean potential temperature pattern at $\sigma_\theta = 14$ clearly identifies the areas of lowest temperatures along the coasts.

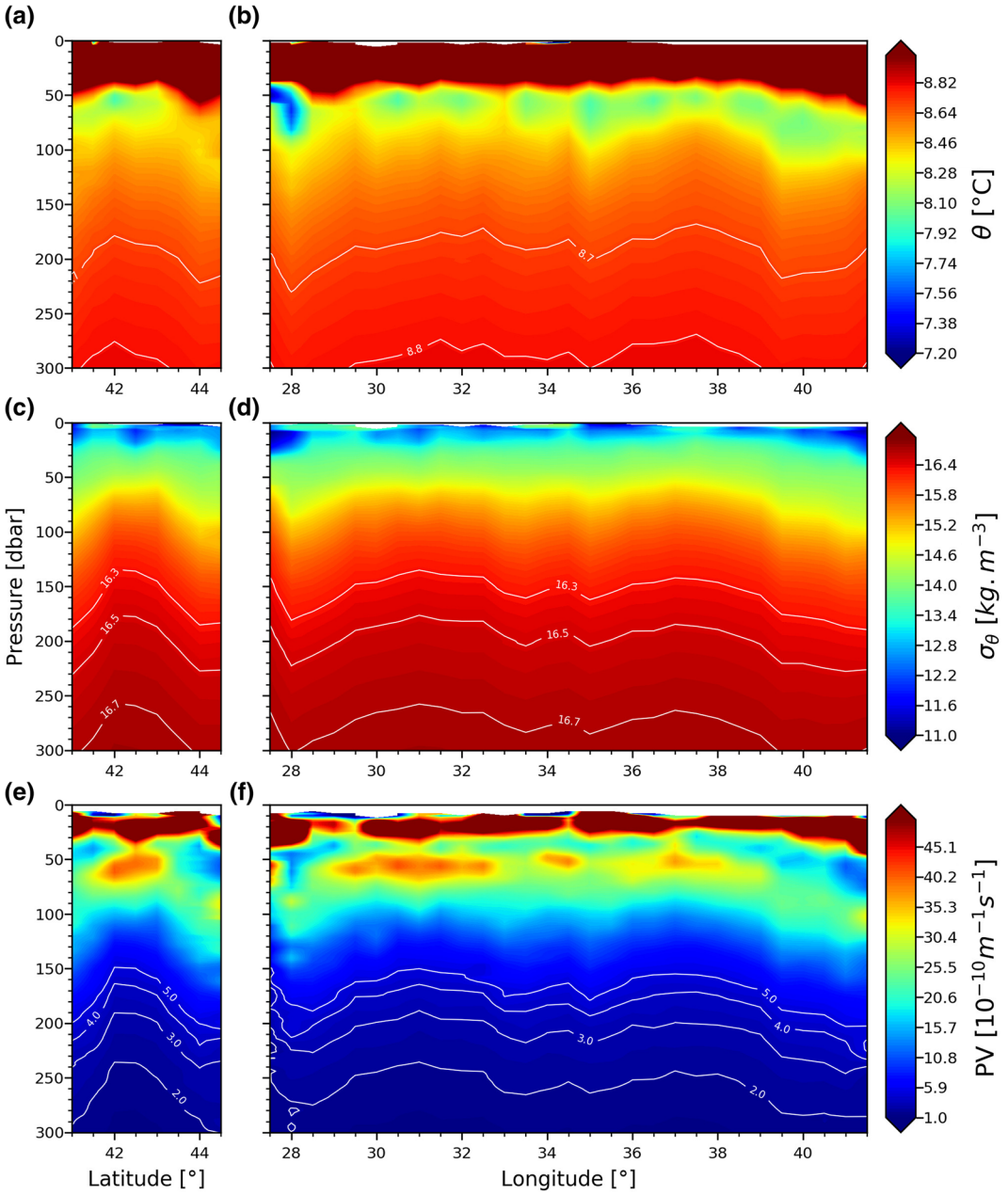

Figure 7. Vertical sections of (a, b) θ, (c, d) σ_θ, and (e, f) PV. The meridional sections are on the left, and the zonal sections are on the right. The respective section lines are shown in Figure 5a. Data used for these plots are collected over areas of 0.75° on both sides of these section lines. PV, potential vorticity.

It seems counterintuitive that in the basin interior, that is, in the area where the isopycnal layers outcrop, the temperature is at the maximum (Figure 6a). The explanation is that (1) the maps in this figure show the annual mean state, and (2) the higher temperatures at $\sigma_\theta = 14$ in the basin interior in winter are due to the upwelling of warmer subsurface waters there (see the dooming of the pycnocline in Figure 7). The analysis of temperature at $\sigma_\theta = 14$ in winter shows the lowest values in the coastal regions west of Crimea and further along the western and southern coast (seasonal maps are shown in Figures S16–S19). There are substantial differences between the patterns shown in Figure 6 and other earlier analyses of historical data. They are explained by the fact that the patterns presented in density coordinates are more informative in terms of isopycnal mixing. The small nonhomogeneity of properties on σ_θ surfaces elucidates how isopycnal

mixing smooths the property distribution between different sources. In contrast, the presentations in geopotential coordinates are more informative in terms of the general circulation.

At $\sim \sigma_\theta = 15$, the range of spatial variability is comparable to the standard deviation over most of the basin area. The difficulty of accurately resolving the horizontal gradients at this isopycnal surface has a physical explanation and reminds us of the well-known fact that in the core of mode waters, temperature is almost homogenous. At the deeper isopycnal levels, there is a clear trend of structuring the horizontal distribution of temperature. The horizontal patterns in Figures 6c and 6d clearly demonstrate the isopycnal pathway of cold water originating from the western coast and propagating eastward. This cooling tends to compensate for the diapycnal warming flux caused by the upwelling of warmer deep water. The intrusions of waters from the Bosporus Strait and the pathway of their eastward propagation along the southern coast are also resolved by the profiling floats (Falina et al., 2017). Knowing that Stanev et al. (2004) performed similar analyses using numerical simulations, one could perceive the results here to be rather obvious. We stress that statistically stable, basin-wide analyses of the isopycnal propagation of water masses based on observational data only became possible due to the unique observations used in the present study.

The distribution of potential temperature, potential density and PV on the vertical meridional and zonal sections (Figure 7) provides a synthesis of the Black Sea thermohaline state over the last 15 years. To increase the statistical credibility of the vertical sections, all data observed at 0.75° north and south of the zonal section line shown in Figure 5a were averaged. The same averaging (east-west) was applied to the meridional section. Profiling floats well captured the dome-shaped pycnocline, the CIL and the pycnostad, the latter is seen as the layer of minimum PV. The near-perfect agreement between the shapes of the CIL and pycnostad in the upper part confirms the similarities between the mode water in the ocean and CIW in the Black Sea. The major difference is the shape of the pycnocline (the panels in the middle), which is convex in the Black Sea and concave in the subtropical gyres. This difference between the ocean and Black Sea cases results from the anticyclonic circulation in the subtropical gyres and cyclonic circulation in the Black Sea.

4. Discussion

The concepts regarding the ventilated thermocline (pycnocline) and isopycnal mixing in the ocean and the Black Sea suggest that wintertime convective mixing, which is due to buoyancy loss from the ocean surface, triggers mode water formation. Cold waters sink down to their neutral density surface and further propagate isopycnally over areas much larger than that of convective sinking. The end result in the ocean is a lateral homogenization of PV caused by isopycnic mixing due to ocean eddies (Rhines & Young, 1982). Large *PV* gradients are only observed in the surface layers, which are directly forced by the wind. One specificity in the Black Sea is the preconditioning role of advective cooling (E. V. Stanev et al., 2003). Another specificity, as shown in the present study, is the cyclonic general circulation, which tends to squeeze the area of low PV between the Rim Current and the coast (or between the Rim Current and the shelf in the North Western Black Sea). This adds to the understanding that the CIW formation varies considerably in the different areas of the Black Sea (E. V. Stanev et al., 2003) and does not operate in the same way as the mode water formation in the subtropical gyres.

The dynamics of Black Sea upper layers provide a classic example of the "connection between climate forcing, physical regime, chemical fluxes, and biological response" (J. W. Murray and Yakushev, 2006; J. W. Murray et al., 2007). In this context, we must remember that the suboxic zone in the Black Sea, which was first discovered by J. W. Murray et al. (1989, see also J. W. Murray 1991), is the interface between the oxic surface layer and sulfidic deep waters. This interface is below the core of the CIL, which overlaps with the layers addressed in the present study. Ventilation of the CIL controls the downward flux of oxygen; therefore, the change in physical state largely affects the biogeochemistry of the Black Sea. As shown by Konovalov and Murray (2001), Stanev et al. (2013), and Capet et al. (2016), the oxygen dynamics reveal clear long-term and interannual changes. Understanding the changing oxic regimes in the Black Sea as a response to changes in its physical system is a fundamental issue of Black Sea oceanography. Changing mixing pathways therefore play a crucial role.

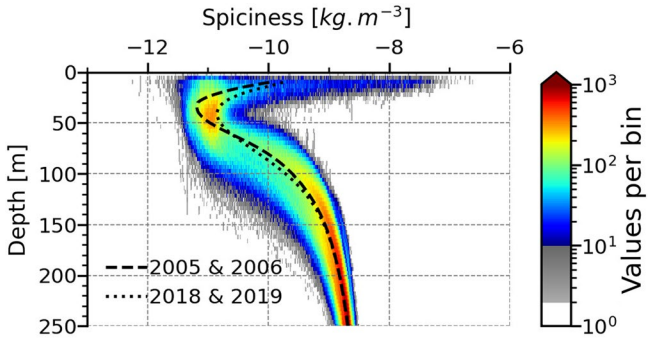

Figure 8. Spiciness in the upper 250 m presented as a function of the number of samples per individual bin. A gray color is used to denote where there are fewer than 10 observations per bin. Bins, in which there are fewer than two observations, are ignored (white in the color bar). Dashed and dotted lines are the means for the first two (2005 and 2006) and last 2 years (2018 and 2019).

In the introduction, we mentioned some of the basic physical processes controlling the formation of CIW. Unfortunately, there are few studies such as that of M. Gregg and Ozsoy (1999) and M. C. Gregg and Yakushev (2005), who used microstructure profiles to quantify such important quantities associated with cold water formation as rates of turbulent dissipation, diapycnal diffusivities, and the depth of ventilation caused by a cold-air outbreak. Further understanding of governing processes has been reached due to ship measurements and numerical modeling, which demonstrated that the injection of cold water into deeper layers is facilitated by mesoscale eddies (Ovchinnikov & Popov, 1987; E. V. Stanev & Staneva, 2001). Zatsepin et al. (2003) also provided evidence that mesoscale eddies contribute to mixing. However, the observational studies mentioned above demonstrated that many fundamental physical quantities cannot be easily measured, particularly over long times and across wide areas.

Data from profiling floats analyzed here provide further evidence of quasi-lateral intrusions associated with intrusions of the Mediterranean water. Such intrusions were previously observed by Stanev et al. (2017), Akpinar et al. (2017), and Falina et al. (2017). These intrusions affect the thermohaline properties of the deeper parts of the CIL, as seen in the anomalies of θ-S profiles (e.g., the autumn 2013 profiles in Figure 4, see also Figures S5–S7). Below the core of the CIL, the role of double diffusion can also be quite significant because salinity stratification has a stabilizing effect on density and temperature stratification has a destabilizing effect. This type of stratification provides the necessary conditions to allow double diffusion. The second condition is that the diffusivity of heat does not equal that of salinity. This is the fundamental difference from the fully developed turbulence, which tends to mix temperature and salinity at equal rates (Radko, 2013).

The profiling floats enable the diagnosis of the oceanographic consequences of water mass formation rather than the quantification of the related short-term processes. Nevertheless, the big data set we presented here appears powerful for quantifying the spatial characteristics of CIW and their changes over the last 15 years, thus providing indirect evidence of the dominant processes. The evolution of the θ-S relationships, which is seen as a continuous flattening of the mixing curves at the base of the CIL after each strong convective event, suggests that the rate of isopycnal mixing at the base of the CIL follows the rate of the diapycnal exchange in the upper layers. Smaller diapycnal mixing (ventilation from above) resulted in smaller isopycnal mixing in the deeper layers (see Williams, 1991, who explained the role of the mixed layer in setting the PV in the ventilated thermocline). This finding could serve as an indication that the pronounced changes in the Black Sea thermohaline state described by Stanev et al. (2019) are controlled by the interplay between diapycnal and isopycnal mixing. These authors attributed the recent thermohaline trends to the warming climate. Additional factors that could reduce the sharpness of the CIL are the change in the θ-S characteristics of the inflow from the Bosporus Strait (including possible changes in the regimes of entrainment and detrainment, Stanev et al., 2004). A small increase in temperature and salinity, which is observed during the recent 15 years below the CIL, will be addressed in more detail in a separate study. This trend allows us to speculate that the consequences of the warming climate are twofold: (1) direct (through air-sea exchange) and (2) indirect (through warm and salty Bosporus intrusions). It seems very plausible that the warming climate affects the CIL by providing warming from above and below. Therefore, the changes in the right end of the θ-S line (corresponding to the deeper layer) need to be carefully considered in the future.

The trend of thermohaline properties of Black Sea water caused by a warming climate is also reflected in the spiciness (Figure 8). To introduce this quantity, we have to go back to the pioneering works of Mamayev (1962) and Stommel (1962), who introduced the idea of a passive thermodynamic variable orthogonal to density. If we denote the differential of density as

$$d\sigma = \beta dS - \alpha d\theta$$

then π, whose differential is

$$d\pi = \beta dS + \alpha d\theta$$

is orthogonal to density $\left(\frac{\partial\sigma}{\partial S} = \frac{\partial\pi}{\partial\theta} \text{ and } \frac{\partial\sigma}{\partial T} = -\frac{\partial\pi}{\partial\theta}\right)$. Later, Munk (Munk, 1981) created the name spiciness (hot and salty) for π, stressing that spiciness gives a measure of the strength of the intrusions (see also Flament, 2002; Veronis, 1972). The results in Figure 8 are produced using the definition of spiciness by T. McDougall and Krzysik (2015) and the open-access Gibbs-Sea Water Oceanographic Toolbox (T. McDougall and Barker 2011).

The case of the Black Sea shows some similarities and differences with the modified Atlantic Waters. The latter is a warm and salty water mass (spicy) with low PV compared to cold and fresh polar waters (Bosse et al., 2018). In the Black Sea, the origin of the spicy water is the Bosporus Strait and the water below the core of CIL is the analog of the polar waters. In both environments, the Black Sea and the Arctic, the density ratio is favorable for diffusive layering because cold and less salty water is above the warmer and saltier water. On the contrary, in large ocean areas of tropical oceans saltier and warmer water is above cold and less salty water, therefore there salt fingers dominate (Radko, 2013; Schmitt, 1994).

Spiciness in the Black Sea combines two important characteristics of stratification. The strongly negative values in the upper layers reflect the core of the CIL. The smooth increase in π below the core corresponds to the upper halocline. Spiciness characterizes density-compensated gradients of temperature and salinity, which are seen as warm water intrusions in Figure 4 and Figures S5–S7. The spread of the θ-S indices (warm and salt against cold and relatively fresh) on izopycnal surfaces is better illustrated in Figure 7 of E. V. Stanev et al. (2019). The difference between the dashed and dotted lines in Figure 8, which gives an estimate of the change in spiciness, demonstrates a response to the warming climate during 2005–2020. Similar indications about regime shifts have been reported by Timmermans and Jayne (2016) for the Arctic, illustrating the relative change of the role temperature. These changes could have profound climatic consequences in the World Ocean and Black Sea.

5. Conclusions

The observations collected from profiling floats contributed substantially to advancing the oceanography of the Black Sea. More than 6,000 profiles were presented and analyzed, revealing the mixing pathways at the base of the CIL and their evolution from 2005 to 2020. It was shown that the CIW has much in common with the mode waters in oceans. For instance, the minimum PV, which in the World Ocean is known as a pycnostad, appeared in the Black Sea at ~40 m, approximately coinciding with the core of the CIL. However, there are numbers of specificities and differences. The horizontal patterns of PV in the ocean are shaped by anticyclonic circulations in the subtropical gyres, while the gyre circulation in the Black Sea is cyclonic, closely following the coast. Therefore, the area of thicker layers with the same density (low PV) in the Black Sea is squeezed between the front and the coast (the shelf in the North Western Black Sea). In the lower part of the CIL, these coastal areas, particularly in the western Black Sea, provide the most important source of cold water propagating further to the east.

The distribution of the individual properties (potential temperature, salinity, etc.) is non-Gaussian when presented in geopotential coordinates and usually has one maximum (just below the core of CIL there are two maxima). It was largely unexpected that the probability distributions presented in density coordinates were completely different, showing several maxima, that is, a "convergence" of thermohaline states along several mixing pathways.

Analyses showed that the CIW is a rather variable end-member with strong interannual variability. The individual "mixing channels" appeared to represent several thermohaline states after several intermittent CIW formation events in the last 15 years. The comparison with earlier observations demonstrated that the density ratio decreased dramatically in the last 25–30 years. During the last 15 years, the mean profile of $R\rho$ also showed a decreasing trend, demonstrating the decreasing role of temperature in the vertical

layering of the Black Sea halocline. The mixing curves at the base of the CIL continuously flattened after each strong convective event (approximately three times for the whole period), manifesting a change in the strength of isopycnal mixing. Furthermore, opposite trends of PV above and below 80 m were observed at the beginning and end of the recent 15-year period, which would suggest opposite changes of the mesoscale dynamics in different layers. The reversal occurs at approximately the depth of $\sigma_\theta = 16$, where the PV is uniform basin-wide with a value of 6.21×10^{10} m^1 s^1. The PV trend would tend to affect the generation and propagation of eddies differently in individual layers, which presumably works in combination with the seasonal changes in PV tending to shape the balance between gyre and eddy circulations.

To test the impact of sampling from profiling floats and exclude possible artifacts, we analyzed the numerical simulations available from the CMEMS operational model of the Black Sea. As a byproduct, it was demonstrated that the model, although assimilating Argo profiles, does not replicate the mixing patterns observed on density levels well. The model θ-S diagrams appeared diffuse; the "mixing channels" did not appear in the model solution. This finding presents a challenge for numerical modelers and indicates that further effort is needed to adequately specify mixing parameterizations, perhaps not only in the Black Sea models. Other possible ocean-wide implications include the changes in the regimes of isopycnal mixing, which might have occurred in other ocean areas. In this respect, the Black Sea could turn out to be a precursor to similar changes occurring in other areas of the world ocean.

Data Availability Statement

Data used in this study are available at http://www.ifremer.fr/co-argoFloats/floatList?detail=false&sort=PTF_CODE%3AASC&active=false&ocean=A&lang=en and https://resources.marine.copernicus.eu/?option=com_csw&view=details&product_id=BLKSEA_ANALYSIS_FORECAST_PHYS_007_001. This research was supported by MASRI – Infrastructure for Sustainable Development of Marine Research of Republic of Bulgaria.

Acknowledgments
The authors thank P.M. Poulain and V. Slabakova for the deployment and technical maintenance of certain floats and E. Peneva for the useful discussions and support. The authors are grateful to the four anonymous reviewers for their constructive comments. This study was supported by the MASRI - Infrastructure for Sustainable Development of Marine Research of Republic of Bulgaria.

References

Akpinar, A., Fach, B. A., & Oguz, T. (2017). Observing the subsurface thermal signature of the Black Sea cold intermediate layer with Argo profiling floats. *Deep Sea Research Part I: Oceanographic Research Papers*, *124*, 140–152. https://doi.org/10.1016/j.dsr.2017.04.002

Badin, G., Williams, R. G., Holt, J., & Fernand, L. J. (2009). Are mesoscale eddies in shelf seas formed by baroclinic instability of tidal fronts?. *Journal of Geophysical Research*, *114*, C10021. https://doi.org/10.1029/2009JC005340

Belokopytov, V. (1998). NATO TU-Black Sea project ecosystem modelling as a management tool. In: L. Ivanov, & T. Oguz (Eds.), *Long-term variability of cold intermediate layer renewal conditions in the Black Sea//NATO ASI ser* (pp. 47–52). Dordrecht: Kluwer Academic Publishers

Belokopytov, V. N. (2011). Interannual variations of the renewal of waters of the cold intermediate layer in the Black Sea for the last decades. *Physical Oceanography*, *20*(5), 347–355. https://doi.org/10.1007/s11110-011-9090-x

Belokopytov, V. N., & Shokurova, I. G. (2005). Estimations of decadal variability in temperature and salinity in the Black Seafor 1951–1995. In: *Ecological safety of coastal and shelf zones and complex use of the shelf resources* (Vol. 12, pp. 12–21). Sevastopol: Marine Hydrophysical Institute

Blatov, A. S., Bulgakov, N. P., Ivanov, V. A., Kosarev, A. N., & Tujilkin, V. S. (1984). In *Variability of hydrophysical fields in the Black Sea* (Vol. 240). Leningrad: Gidrometeoizdat.

Bosse, A., Søiland, H., & Rossby, T. (2018). Fer, I.Atlantic water transformation along its poleward pathway across the Nordic Seas. *Journal of Geophysical Research: Oceans*, *123*, 6428–6448. https://doi.org/10.1029/2018JC014147

Capet, A., Stanev, E. V., Beckers, J.-M., Murray, J., & Gregoire, M. (2016). Decline of the Black Sea oxygen inventory. *Biogeosciences*, *13*(4), 1287–1297. https://doi.org/10.5194/bg-13-1287-2016

Ciliberti, S., Lecci, R., Creti, S., Lemieux-Dudon, B., Lima, L., Storto, A., et al. (2019). User manual for the Black Sea Physics Analysis and Forecast Product. Available at http://resources.marine.copernicus.eu/documents/PUM/CMEMS-BS-PUM-007-001.pdf (Accessed October 15, 2019).

Falina, A., Sarafanov, A., Ozsoy, E., & Turuncoglu, U. U. (2017). Observed basin-wide propagation of Mediterranean water in the Black Sea. *Journal of Geophysical Research: Oceans*, *122*, 3141–3151. https://doi.org/10.1002/2017JC012729

Flament, P. (2002). A state variable for characterizing water masses and their diffusive stability: Spiciness. *Progress in Oceanography*, *54*, 493–501.

Gregg, M., & Ozsoy, E. (1999). Mixing on the Black Sea shelf north of the Bosporus. *Geophysical Research Letters*, *26*, 1809–1872.

Gregg, M. C., & Yakushev, E. (2005). Surface ventilation of the Black Sea's cold intermediate layer in the middle of the western gyre. *Geophysical Research Letters*, *32*, L03604. https://doi.org/10.1029/2004GL021580

Hanawa, K., & Talley, L. D. (2001). Mode waters. Ocean circulation and climate. In G. Siedler, & J. Church (Eds.), *International geophysics series* (pp. 373–386). Academic Press.

Ivanov, V. A., Belokopytov, & , V. N. (2013). *Oceanography of the Black Sea; ECOSY-Gidrofizika; National Academy of Sciences of Ukraine*. Sevastopol: Marine Hydrophysical Institute

Konovalov, S. K., & Murray, J. W. (2001). Variations in the chemistry of the Black Sea on a time scale of decades (1960-1995). *Journal of Marine Systems*, *31*, 217–243.

Konovalov, S. K., Murray, J., & Luther, G. W., III (2005). Basic processes of Black Sea biogeochemistry. *Oceanography*, *18*, 24–35.
Korotaev, G. K., Knysh, V. V., & Kubryakov, A. I. (2014). Study of formation process of cold intermediate layer based on reanalysis of Black-Sea hydrophysical fields for 1971–1993. Izvestiya AN. *Fizika Atmosfery i Okeana*, *50*(1), 35–48.
Korotaev, G., Oguz, T., & Riser, S. (2006). Intermediate and deep currents of the Black Sea obtained from autonomous profiling floats. *Deep-Sea Research Part II*, *53*(17–19), 1901–1910. https://doi.org/10.1016/j.dsr2.2006.04.017
Lee, B. S., Bullister, J. L., Murray, J. W., & Sonnerup, R. E. (2002). Anthropogenic chlorofluorcarbons in the Black Sea and the Sea of Marmara. *Deep-Sea Research Part I*, *49*(5), 895–913. https://doi.org/10.1016/S0967-0637(02)00005-5
Mamayev, O. I. (1962). T-S curves and the vertical stability of ocean waters. *Doklady Akademii Nauk SSSR*, *146*, 227–255.
McCartney, M. S. (1982). The subtropical recirculation of mode waters. *Journal of Marine Research*, *40*, 427–464.
McDougall, T. J. (1984). The relative roles of diapycnal and isopycnal mixing on subsurface water mass conversion. *Journal of Physical Oceanography*, *14*, 1577–1589.
McDougall, T., & Barker, P. (2011). Getting started with TEOS-10 and the Gibbs Seawater (GSW) Oceanographic Toolbox. *SCOR/IAPSO WG*, *127*, 1–28
McDougall, T., & Krzysik, O. (2015). Spiciness. *Journal of Marine Research*, *73*, 141–152. https://doi.org/10.1357/002224015816665589
McWilliams, J. C. (1983). On the mean dynamical balances of the Gulf Stream Recirculation Zone. *Journal of Marine Research*, *41*, 427–460.
Mihailov, M.–. E., Stefan, S., Diakonu, V., & Lazar, L. (2016). Long-term variability of the water mass structure on the Romanian Black Sea Shelf. *Romanian Reports in Physics*, *68*(1), 377–392.
Munk, W. H. (1981). Internal waves and small-scale processes. In B. Warren, & C. Wunsch (Eds.), *Evolution of physical oceanography* (pp. 264–290). Cambridge, MA: The MIT Press.
Murray, J. W. (1991). Hydrographic variability in the Black Sea. In E. Izdar, & J. W. Murray (Eds.), *In Black Sea oceanography*. Kluwer Academic Publishers.
Murray, J. W., Jannasch, H. W., Honjo, S., Anderson, R. F., Reeburgh, W. S., Top, Z., et al. (1989). Unexpected changes in the oxic/anoxic interface in the Black Sea. *Nature*, *338*(6214), 411–413.
Murray, J. W., Stewart, K., Kassakian, S., Krynytzky, M., & DiJulio, D. (2007). Oxic, suboxic, and anoxic conditions in the Black Sea. In V. Yanko-Hombach, A. S. Gilbert, N. Panin, & P. M. Dolukhanov (Eds.), *The Black Sea flood question* (pp. 1–21). Dordrecht: Springer.
Murray, J. W., & Yakushev, E. V. (2006). The suboxic transition zone in the Black Sea. In L. N. Neretin (Ed.), *Past and present water column anoxia. NATO Sciences Series* (pp. 105–138). Springer. https://doi.org/10.1007/1-4020-4297-3_05
Oguz, T., & Besiktepe, S. (1999). Observations on the rim current structure, CIW formation and transport in the western Black Sea. *Deep Sea Research Part I: Oceanographic Research Papers*, *46*(10), 1733–1753. https://doi.org/10.1016/S0967-0637(99)00028-X
Ostrovskii, A. G., & Zatsepin, A. G. (2016). Intense ventilation of the Black Sea pycnocline due to vertical turbulent exchange in the Rim Current area. *Deep-Sea Research Part I*, *116*(1–13), 1–13. https://doi.org/10.1016/j.dsr.2016.07.011
Ovchinnikov, I. M., & Popov, Y. I. (1987). Evolution of the cold intermediate layer in the Black Sea. *Oceanology*, *27*, 555–560.
Ozsoy, E., Unluata, U., & Top, Z. (1993). The evolution of Mediterranean water in the Black Sea: interior mixing and material transport by double diffusive intrusions. *Progress in Oceanography*, *31*, 275–320.
Piotukh, V. B., Zatsepin, A. G., Kazmin, A. S., & Yakubenko, V. G. (2011). Impact of the winter cooling on the variability of the thermohaline characteristics of the active layer in the Black Sea. *Oceanology*, *51*(2), 221–230. https://doi.org/10.1134/S0001437011020123
Provost, C., S. Gana, V. Garc¸on, K. Maamaatuaiahutapu, & M. England (1995), Hydrographic conditions in the Brazil-Malvinas Confluence during austral summer 1990, *Journal of Geophysical Research*, *100*(C6), 10655–10678.
Radko, T. (2013). Double-diffusive convection. *Double-diffusive Convection I-Ii)*. Cambridge, MA: Cambridge University Press.
Rhines, P., & Young, W. (1982). Homogenization of potential vorticity in planetary gyres. *Journal of Fluid Mechanics*, *122*, 347–367. https://doi.org/10.1017/S0022112082002250
Schmitt (1994). Double diffusion in oceanography. *Annual Review of Fluid Mechanics*, *26*, 255–285.
Shapiro, G. I., Stanichny, S. V., & Stanychna, R. R. (2010). Anatomy of shelf-deep sea exchanges by a mesoscale eddy in the North West Black Sea as derived from remotely sensed data. *Remote Sensing of Environment*, *114*(4), 867–875. https://doi.org/10.1016/j.rse.2009.11.020
Shapiro, G. I., Wobus, F., & Aleynik, D. L. (2011). Seasonal and inter-annual temperature variability in the bottom waters over the western Black Sea shelf. *Ocean Science*, *7*(5), 585–596. https://doi.org/10.5194/os-7-585-2011
Staneva, J. V., Dietrich, D., Stanev, E., & Bowman, M. (2001). Rim current and coastal eddy mechanisms in an eddy-resolving Black Sea general circulation model. *Journal of Marine Systems*, *3*, 137–157.
Stanev, E. V., Bowman, M. J., Peneva, E. L., & Staneva, J. V. (2003). Control of Black Sea intermediate water mass formation by dynamics and topography: Comparison of numerical simulations, surveys and satellite data. *Journal of Marine Research*, *61*(1), 59–99. https://doi.org/10.1357/002224003321586417
Stanev, E. V., Grayek, S., Claustre, H., Schmechtig, C., & Poteau, A. (2017). Water intrusions and particle signatures in the Black Sea: A Biogeochemical-Argo float investigation. *Ocean Dynamics*, *67*, 1119–1136. https://doi.org/10.1007/s10236-017-1077-9
Stanev, E. V., He, Y., Grayek, S., & Boetius, A. (2013). Oxygen dynamics in the Black Sea as seen by Argo profiling floats. *Geophysical Research Letters*, *40*, 3085–3090. https://doi.org/10.1002/grl.50606
Stanev, E. V., He, Y., Staneva, J., & Yakushev, E. (2014). Mixing in the Black Sea detected from the temporal and spatial variability of oxygen and sulfide—Argo float observations and numerical modelling. *Biogeosciences*, *11*(20), 5707–5732. https://doi.org/10.5194/bg-11-5707-2014
Stanev, E. V., Le Traon, P.-Y., & Peneva, E. L. (2000). Seasonal and interannual variations of sea level and their dependency on meteorological and hydrological forcing. Analysis of altimeter and surface data for the Black Sea. *Journal of Geophysical Research*, *105*, 17203–17216.
Stanev, E. V., Peneva, E., & Chtirkova, B. (2019). Climate change and regional ocean water mass disappearance: Case of the Black Sea. *Journal of Geophysical Research: Oceans*, *124*, 4803–4819. https://doi.org/10.1029/2019JC015076
Stanev, E. V., Poulain, P.-M., Grayek, S., Johnson, K. S., Claustre, H., & Murray, J. W. (2018). Understanding the dynamics of the oxic-anoxic interface in the Black Sea. *Geophysical Research Letters*, *45*, 864–871. https://doi.org/10.1002/2017GL076206
Stanev, E. V., & Staneva, J. V. (2001). The sensitivity of the heat exchange at ocean surface to meso and sub-basin scale eddies. Model study for the Black Sea. *Dynamics of Atmospheres and Oceans*, *33*(3), 163–189. https://doi.org/10.1016/S0377-0265(00)00063-4
Stanev, E. V., Staneva, J., Bullister, J. L., & Murray, J. W. (2004). Ventilation of the Black Sea pycnocline. Parameterization of convection, numerical simulations and validations against observed chlorofluorocarbon data. *Deep-Sea Research*, *51/12*, 2137–2169.
Stanev, E. V., Staneva, J. V., & Roussenov, V. M. (1997). On the Black Sea water mass formation. Model sensitivity study to atmospheric forcing and parameterization of physical processes. *Journal of Marine Systems*, *13*, 245–272. https://doi.org/10.1016/S0198-0149(10)80009-3
Stanev, E. V. (1990). On the mechanisms of the Black Sea circulation. *Earth-Science Reviews*, *28*(4), 285–319. https://doi.org/10.1016/0012-8252(90)90052-w

Stanev, E. V., Chtirkova, B., & Peneva, E. (2021). Geothermal Convection and Double Diffusion Based on Profiling Floats in the Black Sea. *Geophysical Research Letters*, *48*, e2020GL091788. https://doi.org/10.1029/2020gl091788

Stommel, H. (1962). On the cause of the temperature-salinity curve in the ocean. *Proceedings of the National Academy of Sciences*, *48*, 764–766.

Talley, L. D. (1996). North Atlantic circulation and variability, reviewed for the CNLS Conference. *Physica D*, *98*, 625–646.

Timmermans, M.-L., & Jayne, S. R. (2016). The Arctic Ocean spices up. *Journal of Physical Oceanography*, *46*(4), 1277–1284. https://doi.org/10.1175/JPO-D-16-0027.1

Turgul, S., Basturk, O., Saidam, C., & Yilmaz, A. (1992). Changes in the hydrochemistry of the Black Sea inferred from water density profiles. *Nature*, *359*, 137–139.

Veronis, G. (1972). On properties of seawater defined by temperature, salinity and pressure. *Journal of Marine Research*, *30*, 227–255.

Williams, R. G. (1991). The role of the mixed layer in setting the potential vorticity of the main thermocline. *Journal of Physical Oceanography*, *21*, 1802–1814.

Worthington, L. V. (1959). The 18 water in the Sargasso Sea. *Deep-Sea Research*, *2*, 297–305. https://doi.org/10.1016/0146-6313(58)90026-1

Zatsepin, A. G., Ginzburg, A. I., Kostianoy, A. G., Kremenetskiy, V. V., Krivosheya, V. G., Stanichny, S. V., et al. (2003). Observations of Black Sea mesoscale eddies and associated horizontal mixing. *Journal of Geophysical Research*, *108*(3246), 1–20.

References from the Supporting Information

Argo (2000). *Argo Float Data and Metadata from Global Data Assembly Centre (Argo GDAC)*. SEANOE. https://doi.org/10.17882/42182

Argo data management (2013). Argo users manual. Tech. rep., Ifremer. https://doi.org/10.13155/26387

Wong, A., Keeley, R., Carval, T., & the Argo Data Management Team (2019). *Argo quality control manual for CTD and trajectory data*. Ifremer. https://doi.org/10.13155/33951